membrane type 1 matrix metalloproteinase cleaves the propeptide of progelatinase A and initiates autocatalytic activation. *J. Biol. Chem.* **271,** 17119–17123 (1996).
16. Huovila, A. P., Ilmeida, E. A. C. & White, J. M. ADAMs and cell fusion. *Curr. Opin. Cell Biol.* **8,** 692–699 (1996).
17. Stöcker, W. *et al.* The metzincins: Topological and sequential relations between the astacins, adamalysins, serralysins, and matrixins (collagenases) define a superfamily of zinc-peptidases. *Protein Sci.* **4,** 823–840 (1995).
18. Kessler, E., Takahara, K., Biniaminov, L., Brusel, M. & Greenspan, D. S. Bone morphogenetic protein-1: The type I procollagen C-proteinase. *Science* **271,** 360–362 (1996).
19. Baumann, U., Wu, S., Flaherty, K. M. & McKay, D. B. Three-dimensional structure of the alkaline proteae of *Pseudomonas aeruginosa*: a two-domain protein with a calcium binding parallel β roll motif. *EMBO J.* **12,** 3357–3364 (1993).
20. Bode, W., Gomis-Rüth, F. X., Huber, R., Zwilling, R. & Stöcker, W. Structure of astacin and implications for activation of astacins and zinc-ligation of collagenases. *Nature* **358,** 164–166 (1992).
21. Gomis-Rüth, F. X., Kress, L. F. & Bode, W. First structure of a snake venom metalloproteinase: prototype for matrix metalloproteinases/collagenases. *EMBO J.* **12,** 4151–4157 (1993).
22. Black, R. A. *et al*. A metalloproteinase disintegrin that releases tumour-necrosis factor-α from cells. *Nature* **385,** 729–733 (1997).
23. Moss, M. L. *et al*. Cloning of a disintegrin metalloproteinase that processes precursor tumour-necrosis factor-α. *Nature* **385,** 733–736 (1997).
24. Otwinowski, Z. & Minor, W. *DENZO: A Film Processing for Macromolecular Crystallography* (Yale University, New Haven, CT, 1993).
25. Navaza, J. AMoRe: an automated package for molecular replacement. *Acta crystallogr. A* **50,** 157–163 (1994).
26. Otwinowski, Z. in *Isomorphous Replacement and Anomalous Scattering, Daresbury study weekend proceedings* (SERC Daresbury Laboratory, Warrington, 1991).
27. Cowtan, K. *Joint CCP4 ESF-EACBM Newsletter on Protein Crystallography* Vol. 31 (1994).
28. Roussel, A. & Cambilleau, C. *Turbo-Frodo in Silicon Graphics Geometry, Partners Directory* (Silicon Graphics, Mountain View, CA, 1989).
29. Brünger, A. T. Crystallographic phasing and refinement of macromolecules. *Curr. Opin. Struct. Biol* **1,** 1016–1022 (1991).
30. Nicholls, A., Bharadwaj, R. & Honig, B. Grasp–graphical representation and analysis of surface properties. *Biophys. J.* **64,** 166 (1993).

Acknowledgements. We thank M. Braun for help with crystallization, M. T. Stubbs for reading the manuscript, and A. Lebedev and E. H. Panepucci for help with molecular replacement. This work was supported by the SFB469, the Human Capital and Mobility, and the Biotechnology programs of the European Union, the Fonds der Chemischen Industrie, the BMBF, and the NIH.

Correspondence and requests for materials should be addressed to W.B. (e-mail: bode@biochem.mpg.de). The coordinates have been deposited at the Protein Data Bank (accession no. PDB ID code IUEA).

ER-to-Golgi transport visualized in living cells

John F. Presley, Nelson B. Cole, Trina A. Schroer*, Koret Hirschberg, Kristien J. M. Zaal & Jennifer Lippincott-Schwartz

Cell Biology and Metabolism Branch, National Institute of Child Health and Human Development, Building 18T, NICHD, NIH, Bethesda, Maryland 20892, USA
** Department of Biology, The Johns Hopkins University, Baltimore, Maryland 21218, USA*

Newly synthesized proteins that leave the endoplasmic reticulum (ER) are funnelled through the Golgi complex before being sorted for transport to their different final destinations. Traditional approaches have elucidated the biochemical requirements for such transport[1–3] and have established a role for transport intermediates[4–8]. New techniques for tagging proteins fluorescently[9,10] have made it possible to follow the complete life history of single transport intermediates in living cells, including their formation, path and velocity *en route* to the Golgi complex. We have now visualized ER-to-Golgi transport using the viral glycoprotein ts045 VSVG tagged with green fluorescent protein (VSVG-GFP). Upon export from the ER, VSVG-GFP became concentrated in many differently shaped, rapidly forming pre-Golgi structures, which translocated inwards towards the Golgi complex along microtubules by using the microtubule minus-end-directed motor complex of dynein/dynactin. No loss of fluorescent material from pre-Golgi structures occurred during their translocation to the Golgi complex and they frequently stretched into tubular shapes. Together, our results indicate that these pre-Golgi carrier structures moving unidirectionally along microtubule tracks are responsible for transporting VSVG-GFP through the cytoplasm to the Golgi complex. This contrasts with the traditional focus on small vesicles as the primary vehicles for ER-to-Golgi transport.

VSVG protein from the ts045 mutant strain of vesicular stomatitis virus has been widely used to study membrane transport because of its reversible misfolding and retention in the ER at 40 °C and its ability to move out of the ER and into the Golgi complex upon temperature reduction to 32 °C[11–13]. Green fluorescent protein (GFP)[9,10] was attached to the cytoplasmic tail of VSVG ts045. When expressed in COS cells incubated at 40 °C, VSVG-GFP fluorescence was localized exclusively to the ER (Fig. 1a; 40 °C), a result consistent with the temperature-sensitive folding phenotype of the viral glycoprotein. Upon temperature shift to 32 °C for 15 min the fusion protein redistributed into the juxtanuclear Golgi complex (Fig. 1a; 32 °C) and in biochemical assays[14] became resistant to endo H (data not shown). This time frame for Golgi transport and processing of the fusion protein was indistinguishable from that of untagged VSVG protein in COS cells and was followed by redistribution of VSVG-GFP to the cell surface. Thus, neither the GFP tag nor the imaging of living cells appeared to interfere with the normal folding and transport properties of VSVG.

The initial targets for vesicles budding from the ER *en route* to the Golgi complex are pleiomorphic tubulovesicular structures found in the Golgi region and in peripheral sites[4–8], which are enriched in several proteins (including the COP1 subunit β-COP and ERGIC53)[15–18], and whose proposed function is to concentrate and sort secretory cargo[19,20]. At reduced temperatures (such as 15 °C) these pre-Golgi structures become markedly enlarged and accumulate secretory products[21], presumably owing to a rate-limiting step in membrane transport through these intermediates[22,23]. VSVG-GFP accumulated in such intermediate structures upon incubation for 3 h at 15 °C, co-localizing extensively with β-COP (Fig. 1a; 15 °C) and ERGIC53 (data not shown).

To examine how VSVG-GFP is transported from such intermediates into the Golgi region, cells expressing the chimaeric proteins at 15 °C were placed on a microscope stage warmed to 32 °C and fluorescent images were collected at 3.6-s intervals. As shown in Fig. 1b and c (also see Quicktime movie at http://dir.nichd.nih.gov/CBMB/pb1labob.html), peripheral pre-Golgi structures containing VSVG-GFP translocated rapidly as units into the centrosomal region where they merged into the large fluorescent area marking the Golgi complex. Figure 1b (centre) maps the movement of several of these structures over the course of 9 min upon warm-up from 15 °C to 32 °C. Such structures moved along straight or curvilinear paths towards the cell centre at speeds of up to 1.4 $\mu m\,s^{-1}$. Individual pre-Golgi elements were often greater than 1.5 μm in diameter and frequently changed shape during translocation. Staining of fixed cells with β-COP antibodies during this period revealed the continued association of β-COP and the VSVG-GFP-containing pre-Golgi structures as they clustered inwards to the Golgi complex (data not shown). Inward translocation of two pre-Golgi structures (marked by arrows) is shown in Fig. 1c. A single long tubule was often seen extending in the direction of motion of the pre-Golgi element (Fig. 1b, inset), suggesting that a motor on the tip of the tubule was pulling the mass of pre-Golgi membranes towards the Golgi complex.

Pre-Golgi structures became motile at variable times after warm-up to 32 °C and moved in a stop-and-go fashion toward the Golgi complex. The velocity and path of a single element containing VSVG-GFP, which illustrates this motion, is plotted in Fig. 2a and b. Pre-Golgi structures did not lose fluorescence intensity as they translocated inwards (Fig. 2c), indicating that VSVG-GFP molecules present within them did not bud off into small vesicle carriers, but were carried *en masse* with this structure into the Golgi region.

Cells expressing VSVG-GFP were also visualized upon shifting the temperature directly from 40 °C to 32 °C (Fig. 3a–d and Quicktime movie). Within 1 to 5 min of the shift to lower

temperature, numerous bright fluorescent structures began to appear at widely dispersed sites within the reticular ER labelled by VSVG-GFP (Fig. 3a, arrows). These structures were smaller than the pre-Golgi intermediates observed at 15 °C, but like the 15 °C structures were labelled by antibodies against β-COP (data not shown). When such structures formed, their relative fluorescent intensity was as much as 4 to 10 times above the diffuse fluorescence in the ER (see inset, Fig. 3a). Imaging of the lifetime of these structures revealed that they formed within seconds and stayed at peripheral sites for only brief periods before translocating into the Golgi region (Fig. 3c). Multiple motile structures rarely, if ever, originated sequentially from the same single site but seemed to arise randomly within the ER. Formation and translocation of VSVG-GFP-enriched structures repeatedly occurred until virtually all of the ER-derived fluorescence was redistributed into the Golgi region 15 min after temperature shift (Fig. 3b).

Peripheral pre-Golgi structures containing VSVG-GFP that appeared upon temperature shift from 40 °C to 32 °C translocated rapidly into the Golgi region in a 'stop-and-go' manner, following inward trajectories similar to those of the larger pre-Golgi structures observed during warm-up from 15 °C (Fig. 3c). Movement was not synchronous. At any one time there was a small population of immobile structures. Once a peripheral structure began to move, its fluorescence intensity remained constant. Maximum velocities for movement were around 1.4 μm s^{-1}, similar to velocities of pre-Golgi elements in cells warmed from 15 °C to 32 °C, and consistent

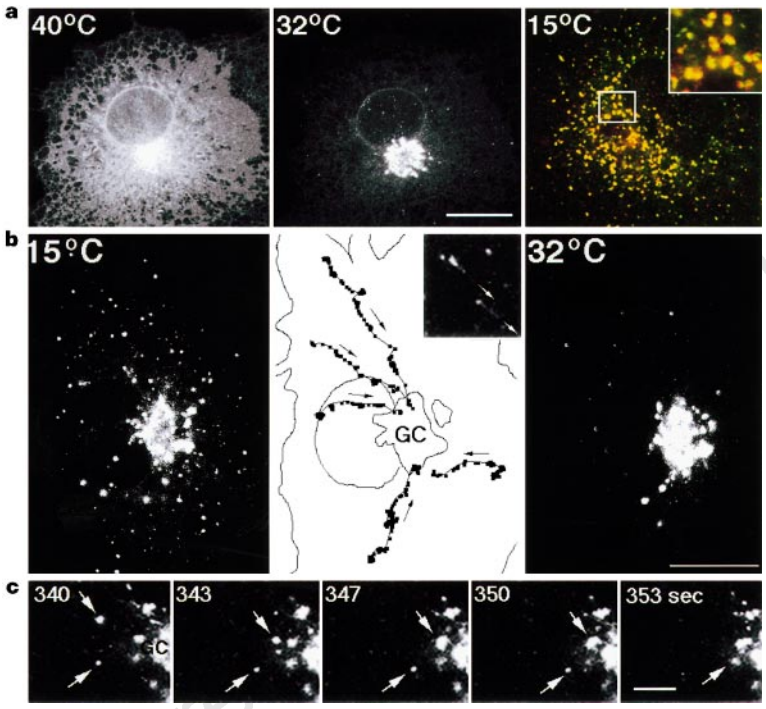

Figure 1 Expression and transport of VSVG-GFP in living cells. **a**, VSVG-GFP expressing COS cells were incubated at 40 °C for 12 h (left panel, 40 °C) and then shifted to 32 °C for 15 min (middle panel, 32 °C) or to 15 °C for 3 h (right panel, 15 °C; fixed (2% formaldehyde) and stained with antibodies to βCOP). The left and middle panels show fluorescence images taken of the same living cell. Green staining in right panel is VSVG-GFP, red staining is βCOP and yellow represents overlap of the two. Scale bar, 20 μm. **b**, VSVG-GFP-expressing COS cells incubated at 15 °C for 3 h and fluorescence images collected at 32 °C. Left panel shows the distribution of VSVG-GFP at the time of warm-up, and right panel shows the distribution 9 min later in the same cell. Paths of pre-Golgi structures are shown in the middle panel (3.5 s intervals). Arrows point in the direction of motion. Inset of middle panel shows high magnification of motile pre-Golgi structure extending a tubule in its direction of movement (marked by arrows). Scale bar, 20 μm. **c**, Image series showing movement of two pre-Golgi structures (see upper and lower arrows) into the Golgi region (GC). Scale bar, 6 μm. (A Quicktime movie sequence from the experiment in **b** is available at http://dir.nichd.nih.gov/CBMB/pb1la-bob.html)

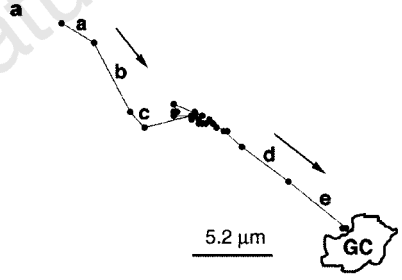

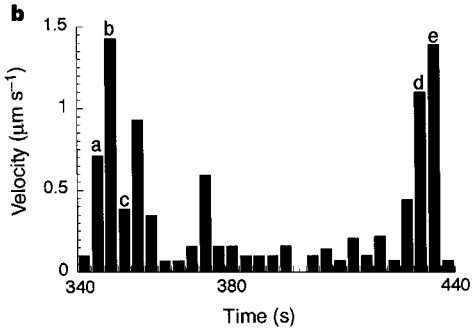

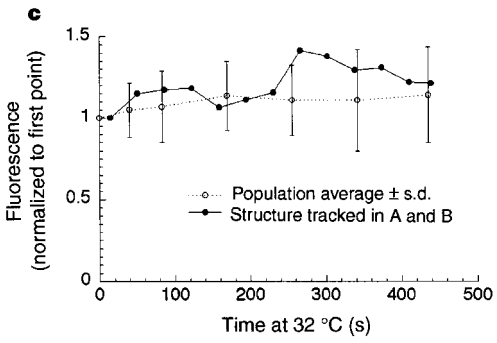

Figure 2 Pathway, velocity and fluorescence intensity of single pre-Golgi structure en route to the Golgi complex. Data are from a single representative cell observed upon warm-up from 15 °C to 32 °C. **a**, Path of a single pre-Golgi intermediate toward the Golgi region. Filled circles show the position of the pre-Golgi intermediate at 3.6-s intervals (100 s total). Arrows show direction of motion. Scale bar, 5.2 μm. **b**, Average velocity of same structure. Filled bars (with letters a–e corresponding to a–e of **a**) mark the average velocity of the pre-Golgi structure during each 3.6-s interval. **c**, Fluorescence intensity of the same structure followed in **a** and **b** (filled circles) and normalized to time 0. Also shown are mean values for the 35 brightest pre-Golgi intermediates in the same cell ± s.d. (empty circles; $n = 9$ at the end of sequence).

with maximal velocities of microtubule-based motors[24]. Extension of tubule processes from a large proportion of the pre-Golgi structures (observed either through the eyepiece of the microscope or in confocal images) indicated these structures were pleiomorphic intermediates rather than single small vesicles (which are incapable of such shape changes) (Fig. 3d). Because virtually every VSVG-GFP-containing pre-Golgi intermediate could be tracked into the Golgi region as an intact unit within a few minutes of its formation (with no significant change in relative fluorescent intensity), VSVG-GFP was carried *en bloc* by these structures to the Golgi complex, as during warm-up from 15 °C. Similar results were found in HeLa, NRK, MDCK, CHO and primary glial cells transfected with VSVG-GFP.

The fate of pre-Golgi structures upon translocation to the Golgi region was observed in cells whose Golgi area was emptied of fluorescence by photobleaching[25] (Fig. 3e and Quicktime movie). Within 5 s to 1 min after photobleaching, pre-Golgi structures began translocating and delivering their contents to the Golgi complex. Within 3 to 5 min of photobleaching, the profile of VSVG-GFP-containing Golgi membranes was similar to the pre-bleach image and there appeared to be no other source than these pre-Golgi structures for delivery of fluorescence. Possible mechanisms for transfer of fluorescence from pre-Golgi structures to the Golgi complex include vesicle budding and fusion, or fusion of whole pre-Golgi structures to the *cis* face of the Golgi complex. No pre-Golgi structures were observed moving back to the cell periphery with any portion of their cargo of VSVG-GFP.

In cells treated with nocodazole to depolymerize microtubules at the time of temperature shift to 32 °C, VSVG-GFP was exported out of the ER into peripheral pre-Golgi elements (Fig. 4a–c). These structures, however, failed to acquire directed motility and remained stationary in the cell periphery (Fig. 4e). Antibody staining of these structures in fixed cells revealed that they contained β-COP and lacked Golgi enzymes (data not shown). Moreover, no significant processing of VSVG-GFP to forms resistant to endo H was observed under these conditions (with less than 5% VSVG-GFP resistant to endo H after 20 min). These results indicate that microtubules are required for translocation of pre-Golgi structures inwards to the cell centre where the Golgi complex normally resides. Upon removal of nocodazole from cells, the peripheral pre-Golgi structures began to move and translocated as individual aggregates following curvilinear trajectories into the cell centre (Fig. 4f).

Over time in cells treated with nocodazole at 32 °C, peripheral pre-Golgi elements containing VSVG-GFP grew increasingly brighter and larger in size (Fig. 4d). This was in contrast to pre-Golgi structures in cells with intact microtubules, whose fluorescence intensity remained constant as they translocated into the Golgi region (Fig. 2c). This difference suggests that pre-Golgi structures in nocodazole-treated cells remain closely associated with ER exit sites where they can continually receive VSVG-GFP and other proteins exported from the ER. Over 1 to 2 h in nocodazole-treated cells, Golgi enzymes slowly redistributed into

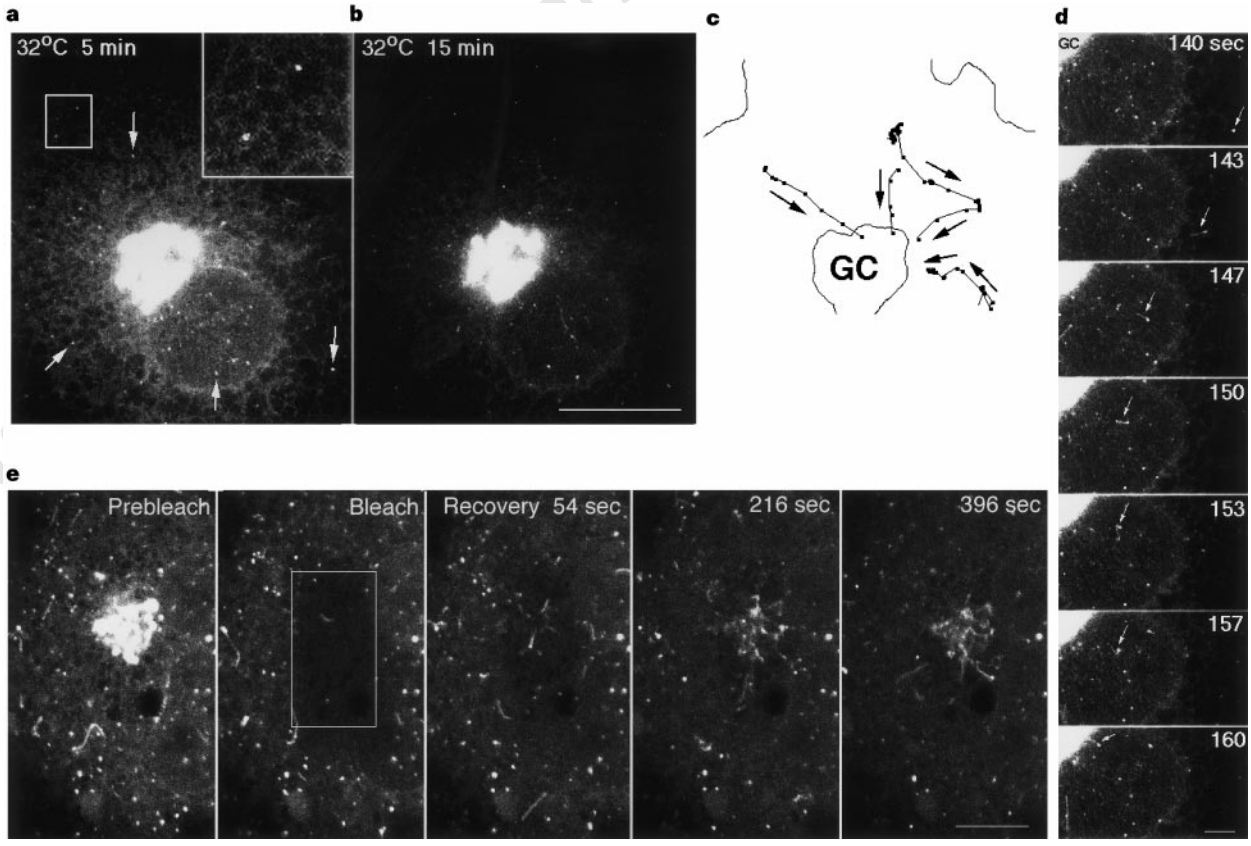

Figure 3 ER to Golgi transport of VSVG-GFP visualized upon shift from 40 °C to 32 °C or in cells whose Golgi area is photobleached. **a**–**d**, VSVG-GFP-expressing COS cells were incubated for 12 h at 40 °C and then shifted to 32 °C. **a**, Distribution of VSVG-GFP after 5 min at 32 °C. Arrows show examples of pre-Golgi intermediates. Inset shows two pre-Golgi structures with fluorescence intensity several fold greater than the ER. **b**, Same cell after 15 min at 32 °C. Scale bar, 20 μm. **c**, Paths taken by several representative pre-Golgi structures en route to the Golgi complex (same cell as in **a** and **b**). Positions shown are at 8.6-s intervals. **d**, Image series showing shape change of a pre-Golgi intermediate as it translocated to the Golgi complex over the time interval shown. Scale bar, 4 μm. **e**, VSVG-GFP-expressing COS cells were incubated for 12 h at 40 °C, shifted to 15 °C for 3h and then warmed to 32 °C. Fluorescence associated with the Golgi complex was photobleached with high-intensity laser light and subsequent inward delivery of VSVG-GFP from pre-Golgi intermediates followed over the time periods indicated. Scale bar, 9.6 μm.

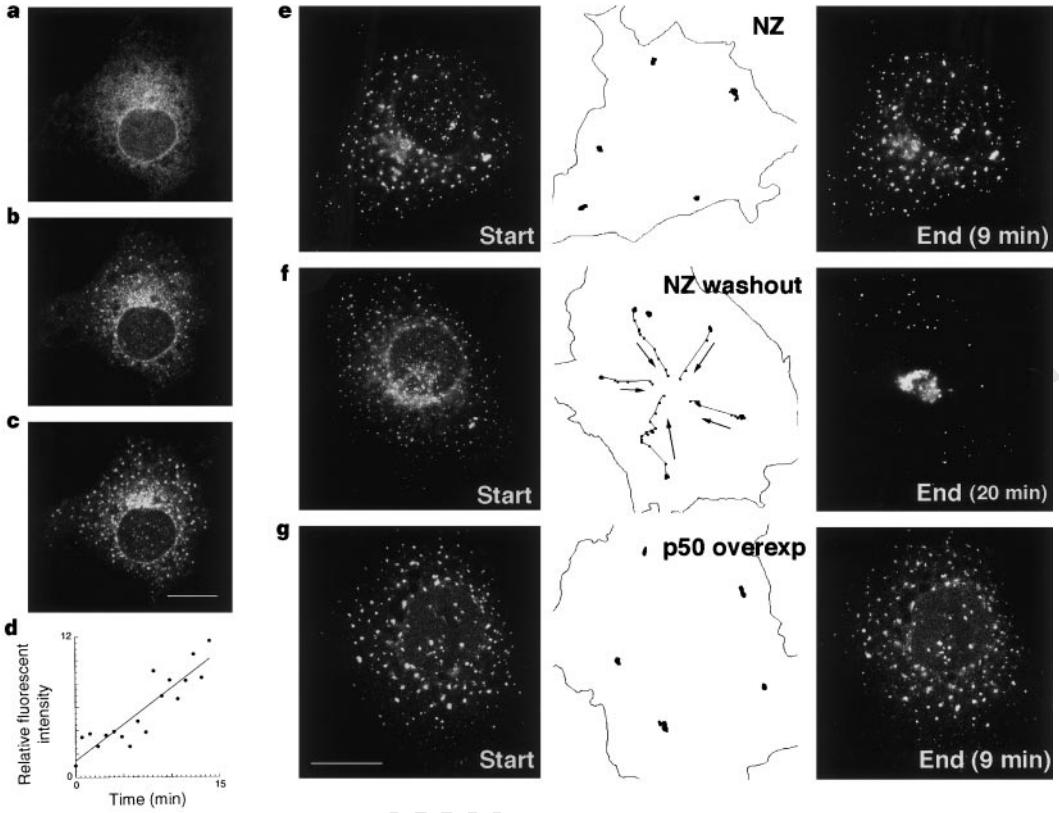

Figure 4 Role of microtubules and dynein/dynactin in translocation of pre-Golgi structures. **a**–**c**, COS cells expressing VSVG-GFP at 40 °C were placed on ice for 15 min with 1 μg ml^{-1} nocodazole, and warmed to 32 °C in the presence of drug. Images were collected at 0 min (**a**), 10 min (**b**) and 20 min (**c**) at 32 °C. Scale bar, 20 μm. **d**, Fluorescence intensity of pre-Golgi structure in nocodazole-treated cell from image sequences collected at 3.6-s intervals at 32 °C. **e**–**g**, Path of pre-Golgi structures in cells in which VSVG-GFP was accumulated in the ER at 40 °C and then images taken at 10-s intervals at 32 °C under different conditions. 'Start' shows the distribution of VSVG-GFP at the beginning of the sequence, 'End' shows the distribution 9 or 20 min later. Middle panels show the path of structures tracked over the period between 'start' and 'end'. **e** shows a 9-min sequence of a cell treated with nocodazole as in **a** and images taken starting after 20 min in the drug. **f** shows a 20-min sequence of a cell treated with nocodazole as in **e** and then washed free of the drug. **g**, A 9-min sequence of a cell co-expressing VSVG-GFP and dynamitin beginning after 10 min at 32 °C. A Quicktime movie sequence of **e**–**g** is available (see Fig. 1 legend).

the peripheral structures containing VSVG-GFP (data not shown), leading to reformation of Golgi stacks at ER exit sites as previously described[14].

The loss of motility of pre-Golgi elements after microtubule disruption with nocodazole suggested that a microtubule motor protein powers their inward movement. Consistent with this, energy depletion with deoxyglucose and azide blocked their inward translocation (data not shown). Cytoplasmic dyneins are minus-end-directed, microtubule-dependent ATPases involved in organelle motility. At least one isoform of cytoplasmic dynein[31] (dynein 1) interacts with dynactin[26,27], another multisubunit complex, to target subcellular organelles to microtubules. To inhibit dynein activity, we overexpressed the p50/dynamitin subunit of dynactin in VSVG-GFP-expressing cells. Overexpression of dynamitin disrupts the dynactin complex and dissociates both it and cytoplasmic dynein from mitotic kinetochores[28]. It also results in dispersion of the Golgi complex, presumably because of a role of dynein/dynactin in Golgi positioning[29]. As shown in Fig. 4g, VSVG-GFP-containing peripheral structures failed to translocate into the centrosomal region upon shift from 40 °C to 32 °C in cells overexpressing dynamitin and remained as stationary structures in the cell periphery even though microtubules were intact. This inhibitory effect occurred before the effects of dynamitin on Golgi fragmentation (not shown) and suggested that translocation of peripheral pre-Golgi structures inwards along microtubules is powered by the microtubule motor complex of dynein/dynactin.

In summary, use of VSVG-GFP chimaeras to follow membrane transport in living cells has revealed new information about the nature and lifetime of transport intermediates involved in membrane traffic between the ER and Golgi complex. VSVG-GFP rapidly emerged from the ER at multiple peripheral sites, resulting in the accumulation of chimaeric protein in numerous peripheral membrane structures. These structures translocated as units along microtubules into the Golgi region without loss of accumulated VSVG-GFP, and were often large enough to deform in shape during transport, suggesting they are non-vesicular membrane transport intermediates. The data further underscore the importance of microtubules and microtubule-based motors: pre-Golgi transport intermediates required microtubules to translocate inwards to the Golgi complex and appeared to use the dynein/dynactin motor complex for this purpose. □

Methods

Cloning and expression of VSVG-GFP. VSVG-GFP was generated by fusing enhanced GFP (Clontech, Palo Alto, CA) directly after the final amino acid of the carboxy terminus of VSVG ts045 (ref. 30; provided by J. Rose) by standard two-stage polymerase chain reaction (PCR) cloning methods. The construct was cloned into the CMV promoter-driven expression plasmid, pCDM8.1 (Invitrogen), and transiently expressed in COS cells by electroporation.

Fluorescence imaging. GFP-expressing cells were imaged at 32 °C in buffered medium with a Zeiss LSM 410 confocal microscope system having a ×100 Zeiss planapo objective (NA1.4) or with a microscope equipped with a cooled charge-coupled device (CCD) system described in ref. 14. Detectors on both microscopes gave a linear response to light under the conditions in this study.

Small 50–100 nm structures (vesicles) can easily be detected with our imaging system given the presence of enough fluorescent signal (we can visualize coated pits or caveolae using fluorescent antibody labelling). Line averaging rather than frame averaging was used in confocal imaging (images were acquired with a single top-to-bottom scan) to prevent artefacts caused by movement during data acquisition. Temperature was controlled using a Nevtek air stream stage incubator (Bursville). The GFP molecule was excited with the 488 line of a krypton-argon laser and the images made with a 515-540 bandpass filter. Images were processed using NIH image software (Wayne Rasband Analytics, NIH) and were printed with a Fujix Pictrography 3000 digital printer.

Fluorescence intensity of pre-Golgi intermediates formed at 15 °C was measured by centering on a circular region of interest 6 pixels in diameter (1 pixel = 0.26 μm in the source images for Fig. 2) on the brightest point of the punctate pre-Golgi intermediate in each image and measuring the total fluorescence in this region. If this region was insufficient to surround the apparent area of the pre-Golgi intermediate in the first frame completely, a larger region was used for the first and kept constant for subsequent frames. A nearby background region of equal area was similarly measured and subtracted. Background pixel values were <20% of the average intensity of these structures. Fluorescence intensity was normalized to the first time point.

Received 21 March; accepted 16 June 1997.

1. Rothman, J. E. & Wieland, F. T. Protein sorting by transport vesicles. *Science* **272,** 227–234 (1996).
2. Schekman, R. & Orci, L. Coat proteins and vesicle budding. *Science* **271,** 1526–1533 (1996).
3. Aridor, M., Bannykh, S., Rowe, T. & Balch, W. E. Sequential coupling between CopII and CopI vesicle coats in endoplasmic reticulum to Golgi transport. *J. Cell Biol.* **131,** 1–19 (1995).
4. Pluttner, H., Davidson, H. W., Saraste, J. & Balch, W. E. Morphological analysis of protein transport from the ER to Golgi membranes in digitonin-permeabilized cells: role of the p58 containing compartment. *J. Cell Biol.* **119,** 1097–1116 (1992).
5. Saraste, J. & Svensson, K. Distribution of the intermediate elements operating in ER to Golgi transport. *J. Cell Sci.* **100,** 415–430 (1991).
6. Saraste, J. & Kuismanen, E. Pathways of protein sorting and membrane traffic between the rough endoplasmic reticulum and the Golgi complex. *Semin. Cell Biol.* **3,** 343–355 (1992).
7. Krijnse-Locker, J., Ericsson, M., Rottier, P. J. & Griffiths, G. Characterization of the budding compartment of mouse hepatitis virus: Evidence that transport from the RER to the Golgi complex requires only one vesicular transport step. *J. Cell Biol.* **124,** 55–70 (1994).
8. Stinchcombe, J. C., Nomoto, H., Cutler, D. F. & Hopkins, C. R. Anterograde and retrograde traffic between the rough endoplasmic reticulum and the Golgi complex. *J. Cell Biol.* **131,** 1387–1401 (1995).
9. Prasher, D. C., Eckenrode, V. K., Ward, W. W., Prendergast, F. G. & Cormier, M. J. Primary structure of the Aequorea victoria green-fluorescent protein. *Gene* **111,** 229–233 (1992).
10. Chalfie, M., Tu, Y., Euskirchen, G., Ward, W. W. & Prasher, D. C. Green fluorescent protein as a marker for gene expression. *Science* **263,** 802–805 (1994).
11. Kreis, T. E. & Lodish, H. F. Oligomerization is essential for transport of vesicular stomatitis viral glycoprotein to the cell surface. *Cell* **46,** 929–937 (1986).
12. Beckers, C. J., Keller, D. S. & Balch, W. E. Semi-intact cells permeable to macromolecules: Use in reconstitution of protein transport from the endoplasmic reticulum to the Golgi complex. *Cell* **50,** 523–534 (1987).
13. Bergmann, J. E. Using temperature-sensitive mutants of VSV to study membrane protein biogenesis. *Methods Cell Biol.* **32,** 85–110 (1989).
14. Cole, N. B., Sciaky, N., Marotta, A., Song, J. & Lippincott-Schwartz. J. Golgi dispersal during microtubule disruption: regeneration of Golgi stacks at peripheral endoplasmic reticulum exit sites. *Mol. Biol. Cell* **7,** 631–650 (1996).
15. Schweizer, A., Fransen, J. A. M., Bachi, T., Ginsel, L. & Hauri, H.-P. Identification, by a monoclonal antibody, of a 53 kD protein associated with a tubulo-vesicular compartment at the cis-side of the Golgi apparatus. *J. Cell Biol.* **107,** 1643–1653 (1988).
16. Lippincott-Schwartz, J., Cole, N. B., Marotta, A., Conrad, P. A. & Bloom, G. S. Kinesin is the motor for microtubule-mediated Golgi-to-ER membrane traffic. *J. Cell Biol.* **128,** 293–306 (1995).
17. Pepperkok, R. *et al.* βCOP is essential for biosynthetic membrane transport from the endoplasmic reticulum to the Golgi complex *in vivo*. *Cell* **74,** 71–82 (1993).
18. Peter, F., Plutner, H., Zhu, H., Kreis, T. E. & Balch, W. E. β-COP is essential for transport of protein from the endoplasmic reticulum to the Golgi *in vitro*. *J. Cell Biol.* **122,** 1155–1168 (1993).
19. Balch, W. E., McCaffery, J. M., Pluttner, H. & Farquhar, M. G. Vesicular stomatitis virus is sorted and concentrated upon exit from the endoplasmic reticulum. *Cell* **76,** 841–852 (1994).
20. Bannykh, S. I., Rowe, T. & Balch, W. E. The organization of endoplasmic reticulum export complexes. *J. Cell Biol.* **135,** 19–35 (1996).
21. Kuismanen, E. & Saraste, J. Low temperature-induced transport blocks as tools to manipulate membrane traffic. *Methods Cell Biol.* **32,** 257–274 (1989).
22. Hauri, H.-P. & Schweizer, A. The endoplasmic reticulum–Golgi intermediate compartment. *Curr. Opin. Cell Biol.* **4,** 600–608 (1992).
23. Lotti, L. V., Torrisi, M. R., Pascale, M. C. & Bonatti, S. Immunocytochemical analysis of the transfer of vesicular stomatitis virus G glycoprotein from the intermediate compartment to the Golgi complex. *J. Cell Biol.* **118,** 43–50 (1992).
24. Walker, R. A. & Sheetz, M. P. Cytoplasmic microtubule-associated motors. *Annu. Rev. Biochem.* **62,** 429–451 (1993).
25. Cole, N. B. *et al.* Diffusional mobility of Golgi proteins in membranes of living cells. *Science* **273,** 797–801 (1996).
26. Schroer, T. A., Bingham, J. B. & Gill, S. R. Actin-related protein 1 and cytoplasmic dynein-based motility: What's the connection? *Trends Cell Biol.* **6,** 212–215 (1996).
27. Gaglio, T. *et al.* Opposing motor activities are required for the organization of the mammalian mitotic spindle pole. *J. Cell Biol.* **135,** 399–414 (1996).
28. Echeverri, C. J., Paschal, B. B., Vaughan, K. T. & Vallee, R. B. Molecular characterization of the 50-kD subunit of dynactin reveals function for the complex in chromosome alignment and spindle organization during mitosis. *J. Cell Biol.* **132,** 617–633 (1996).
29. Burkhardt, J. K., Echeverri, C. J. & Vallee, R. B. Overexpression of the p50 subunit of dynactin perturbs the positioning of the Golgi apparatus and endosomes. *Mol. Biol. Cell* **6,** 266a (1995).
30. Gallione, C. J. & Rose, J. K. A single amino acid substitution in a hydrophobic domain causes temperature-sensitive cell-surface transport of a mutant viral glycoprotein. *J. Virol.* **54,** 374–382 (1985).
31. Vaisberg, E. A., Grissom, P. M. & McIntosh, J. R. Mammalian cells express three distinct dynein heavy chains that are localized to different cytoplasmic organelles. *J. Cell Biol.* **133,** 831–842 (1996).

Acknowledgements. We thank R. Klausner, E. Siggia, J. Bonifacino, C. Smith, J. Donaldson, J. Ellenberg and R. Stearman for valuable comments and suggestions, and J. Rose for his generous gift of reagent.

Correspondence and requests for materials should be addressed to J.L.-S. (e-mail: jlippin@helix.nih.gov).

Smad4 and FAST-1 in the assembly of activin-responsive factor

Xin Chen, Ellen Weisberg, Valerie Fridmacher, Minoru Watanabe, Grace Naco & Malcolm Whitman

Department of Cell Biology, Harvard Medical School, 240 Longwood Avenue, Boston, Massachusetts 02115-5730, USA

Members of the TGF-β superfamily of signalling molecules work by activating transmembrane receptors with phosphorylating activity (serine–threonine kinase receptors)[1]; these in turn phosphorylate and activate[2] SMADs[3,4], a class of signal transducers. Activins are growth factors that act primarily through Smad2[5–7], possibly in partnership with Smad4, which forms heteromeric complexes with different ligand-specific SMADs after activation[8,9]. In frog embryos, Smad2 participates in an activin-responsive factor (ARF), which then binds to a promoter element of the *Mix.2* gene[10]. The principal DNA-binding component of ARF is FAST-1 (ref. 11), a transcription factor with a novel winged-helix structure. We now report that Smad4 is present in ARF, and that FAST-1, Smad4 and Smad2 co-immunoprecipitate in a ligand-regulated fashion. We have mapped the site of interaction between FAST-1 and Smad2/Smad4 to a novel carboxy-terminal domain of FAST-1, and find that overexpression of this domain specifically inhibits activin signalling. In a yeast two-hybrid assay, the FAST-1 carboxy terminus interacts with Smad2 but not Smad4. Deletion mutants of the FAST-1 carboxy terminus that still participate in ligand-regulated Smad2 binding no longer associated with Smad4 or ARF. These results indicate that Smad4 stabilizes a ligand-stimulated Smad2–FAST-1 complex as an active DNA-binding factor.

Smad2 associates in a ligand-regulated manner with another member of the Smad family, Smad4 (ref. 8). To test whether Smad4 is a component of ARF, we expressed epitope-tagged Smad4 by injection of messenger RNA into 2-cell embryos either with or without co-injection of activin mRNA; we then tested whether ARF isolated from these embryos at stage 9 could be supershifted in an electrophoretic mobility-shift assay (EMSA) by incubation with anti-tag antibody (Fig. 1a). In this assay, Smad4 was incorporated into ARF, but overexpression of Smad4 was insufficient to stimulate ARF formation in the absence of ligand activation (Fig. 1a, lanes 2 and 3).

Incorporation of Smad4 into ARF could reflect either the association of Smad2, Smad4 and FAST-1 into the same complex, or the formation of two distinct types of ARF: Smad2-containing ARF and Smad4-containing ARF. To distinguish between these possibilities, we overexpressed Smad2 bearing a Myc-epitope tag and Smad4 bearing a haemagglutinin (HA) epitope tag, and did an EMSA supershift with each anti-tag antibody alone or together. Addition of both anti-tag antibodies supershifted ARF-containing tagged Smad4 and Smad2 to a position higher than either antibody alone (Fig. 1b), indicating that Smad2 and Smad4 are present in the same complex, rather than in two discrete subsets of ARF complexes.